Dynamical matching in a three-dimensional Caldera potential-energy surface

Stephen Wiggins [1,2,*] and Matthaios Katsanikas [3,1,2,†]

[1] *School of Mathematics, University of Bristol, Fry Building, Woodland Road, Bristol BS8 1UG, United Kingdom*

[2] *Department of Mathematics, United States Naval Academy, Chauvenet Hall, 572C Holloway Road, Annapolis, Maryland 21402-5002, USA*

[3] *Research Center for Astronomy and Applied Mathematics, Academy of Athens, Soranou Efesiou 4, Athens GR-11527, Greece*

(Received 4 January 2023; accepted 8 June 2023; published 19 July 2023)

In a previous paper, we used a recent extension of the periodic-orbit dividing surfaces method to distinguish the reactive and nonreactive parts in a three-dimensional (3D) Caldera potential-energy surface. Furthermore, we detected the phenomenon of dynamical matching in a 3D Caldera potential-energy surface. This happened for a specific value of the radius r of the periodic orbit dividing surfaces ($r = 0.25$). In this paper, we demonstrated that the chemical ratios of the number of reactive and nonreactive trajectories to the total number of trajectories converges for a range of the radius r of the periodic-orbit dividing surfaces. This is important not only for validating the previous paper and to confirm that the method can detect the phenomenon of dynamical matching independently of the chosen radius of the construction of the dividing surface but also for investigating the application of the method to other Hamiltonian models.

DOI: 10.1103/PhysRevE.108.014206

I. INTRODUCTION

The classical Caldera potential is a two-dimensional (2D) potential-energy surface (PES) introduced by Carpenter [1,2] in his development of the concept of dynamical matching in reactions of organic molecules. Since then the Caldera PES has been used to describe a variety of organic molecular reactions, such as the vinylcyclopropane-cyclopentene rearrangement [3,4], the stereomutation of cyclopropane [5], and the degenerate rearrangement of bicyclo[3.1.0]hex-2-ene [6,7] or that of 5-methylenebicyclo[2.1.0]pentane [8].

The original Caldera PES has a well that is surrounded by four index-1 saddle points. The two higher-energy index-1 saddles correspond to the reactants and the two lower-energy index-1 saddles correspond to the products (see, for example, Ref. [9]). As we remarked above, an interesting phenomenon is the dynamical matching (see Refs. [1,9]). Dynamical matching means that all trajectories that enter the Caldera region by crossing the higher-energy index-1 saddles go straight across the Caldera and exit through the region of the opposite lower-energy index-1 saddle.

Dividing surfaces provide a method of monitoring the passage of trajectories between qualitatively distinct regions of the phase space. It is important that these dividing surfaces are phase-space objects since the nature of the trajectories will generally change as the total energy is varied. The construction of such phase-space dividing surfaces for 2 degrees-of-freedom Hamiltonian systems using an unstable periodic orbit ("periodic-orbit dividing surfaces") was pioneered by Pechukas, Pollak, and co-workers in Refs. [10–15].

The phenomenon of dynamical matching has been studied for 2D Caldera PES using dividing surfaces (see Refs. [16,17]) and the method of Lagrangian descriptors ([18,19]. Studies of dynamical matching in the Caldera PES after symmetry breaking and/or bifurcation of the critical points of the PES have been carried out in Refs. [17–21].

We note that all of these studies of dynamical matching have been carried out for 2D Caldera PES. In this work, we consider an extension of the 2D symmetric Caldera potential-energy surface coupling the axis of symmetry of this potential with a harmonic oscillator in the z direction. Recently, we have constructed an alternative method to construct dividing surfaces in Hamiltonian systems with 3 or more degrees of freedom without knowing the. normal hyperbolic invariant manifold (NHIM) (avoiding the extensive and difficult calculations of normal form theory—see, for example, Refs. [22–26]). We used the periodic orbit, which is actually a one-dimensional submanifold of the normally hyperbolic invariant manifold, as a starting point to construct a dividing surface [27,28]. We constructed a torus using as a basis a periodic orbit and we extended this to a $(2n-2)$-dimensional object in the $(2n-1)$-dimensional energy surface. We illustrated our methods using benchmark examples for 2 and 3 degrees of freedom Hamiltonian systems to demonstrate the corresponding algorithm for this construction. We proved that this object was a dividing surface and it has the no-recrossing property. For the construction of these objects, in all of our previous work we used a fixed value of radius r. This value of r is not arbitrary but it has a range of values with a maximum (see Refs. [27,28]). This maximum was computed in the benchmark examples (integrable models) that we used in these papers very easily. Subsequently we applied, for the first time, this method to detect the phenomenon of dynamical

*s.wiggins@bristol.ac.uk

†mkatsan@academyofathens.gr

TABLE I. Critical points of the Caldera potential for $c_1 = 5$, $c_2 = 3$ $c_3 = -0.3$, $c_4 = 0.2$, and $c_5 = 0.03$ (RH and LH are the abbreviations for right hand and left hand, respectively).

Critical point	x	y	z	E
Central minimum	0.000	−0.297	0	−0.448
Upper LH saddle	−2.149	2.0778	0	27.0123
Upper RH saddle	2.149	2.0778	0	27.0123
Lower LH saddle	−1.923	−2.003	0	14.767
Lower RH saddle	1.923	−2.003	0	14.767

matching in a nonintegrable Hamiltonian model (like that of a Caldera-type Hamiltonian model) for a fixed value of energy using a fixed value of radius r. In that case, we could not compute the maximum value of that radius analytically, and this means that the interval of the radius $[0, r_{\max}]$ is unknown. A natural question that arises after this paper is what is the effect of changing the radius on the dynamical phenomena that we observed for a fixed radius? The investigation of this restriction for nonintegrable cases of Hamiltonian systems is an interesting topic, and is the subject of this paper. Possible effects of the change of radius could be a change of dynamical behavior or the convergence of the radius for the different types of trajectory behavior. This is important not only for validating the previous paper and to confirm that the method can detect this phenomenon independently of the chosen radius of the construction of the dividing surface, but to investigate the application of the method to other Hamiltonian models. This will allow us to detect and investigate other chemical phenomena and in general in all fields where we have applications of the transition state theory (dividing surfaces play a central role in the transition state theory [24,29]) and dynamical astronomy (see Ref. [30]). Hence this paper not only complete the previous study (see Ref. [31]) but it satisfies the general aim of investigating the manner in which this method will be applied in the future, answering a variety of important questions from many fields of nonlinear dynamics.

In the next section (Sec. II), we describe our model. Then we present our results (Sec. III) and our conclusions (Sec. IV).

II. MODEL

The potential of our model is the Caldera potential plus two terms that correspond to a harmonic oscillator in the z direction ($c_4 z^2$) and the coupling term ($c_5 y z^2$):

$$V(x, y, z) = c_1(x^2 + y^2) + c_2 y - c_3(x^4 + y^4 - 6x^2y^2) + c_4 z^2 + c_5 y z^2, \quad (1)$$

where (x, y, z) are Cartesian coordinates. For the parameters of the Caldera we have $c_1 = 5$, $c_2 = 3$, and $c_3 = -0.3$ (see Refs. [9,16–19]) and for the parameters of the other two terms we use the values $c_4 = 0.2$ and $c_5 = 0.03$. The positions of the critical points are given in Table I. As we can see in Fig. 1, the 2D topography of this potential is similar to that of the 2D Caldera potential (see Refs. [9,16,18]). The difference is that the walls of this potential extend the potential walls of the 2D Caldera into the z direction. It can be considered as a natural 3D extension of the corresponding 2D Caldera. The

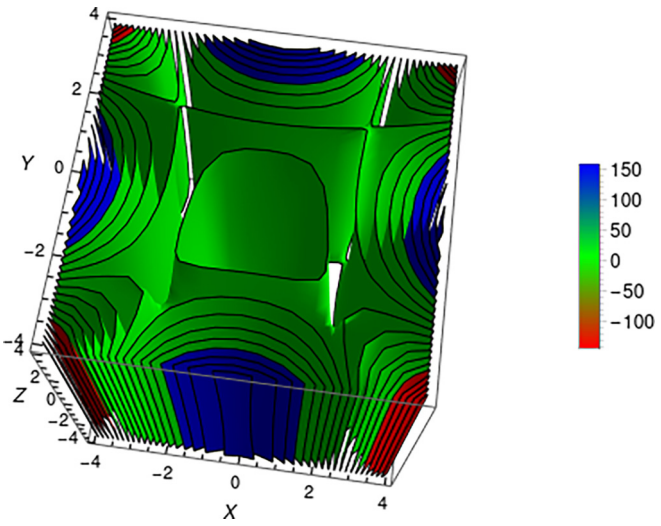

FIG. 1. The contours of the 3D Caldera potential.

corresponding Hamiltonian is

$$H(x, y, p_x, p_y) = \frac{p_x^2}{2m} + \frac{p_y^2}{2m} + \frac{p_z^2}{2m} + V(x, y, z), \quad (2)$$

where $V(x, y, z)$ is the potential and p_x, p_y, and p_z are the corresponding momenta ($m = 1$). The equations of motion are given by

$$\begin{aligned}
\dot{x} &= \frac{\partial H}{\partial p_x} = \frac{p_x}{m}, \\
\dot{y} &= \frac{\partial H}{\partial p_y} = \frac{p_y}{m}, \\
\dot{y} &= \frac{\partial H}{\partial p_z} = \frac{p_z}{m}, \\
\dot{p_x} &= -\frac{\partial V}{\partial x}(x, y, z) = -(2c_1 x - 4c_3 x^3 + 12c_3 x y^2), \\
\dot{p_y} &= -\frac{\partial V}{\partial y}(x, y, z) \\
&= -(2c_1 y - 4c_3 y^3 + 12c_3 x^2 y + c_2 + c_5 z^2), \\
\dot{p_z} &= -\frac{\partial V}{\partial y}(x, y, z) = -(2c_4 z + 2c_5 y z). \quad (3)
\end{aligned}$$

III. RESULTS

In a previous paper (see Ref. [31]), we constructed the dividing surfaces from unstable periodic orbits of the higher-energy upper-right index-1 saddle for a specific value of the radius of this surface, $r = 0.25$ (for the value of energy $E = 28$). In this section, we construct the dividing surfaces from unstable periodic orbits of the higher-energy upper-right index-1 saddle for $r = 0.1$ and $r = 0.4$ (for the same value of energy). The results will be the same for the case of the other upper index-1 saddle because of the symmetry of the potential. Using this method, we have as a basis the projection (y, p_y) of the periodic orbits of the family of unstable periodic orbits of the upper index-1 saddles. This projection is a closed

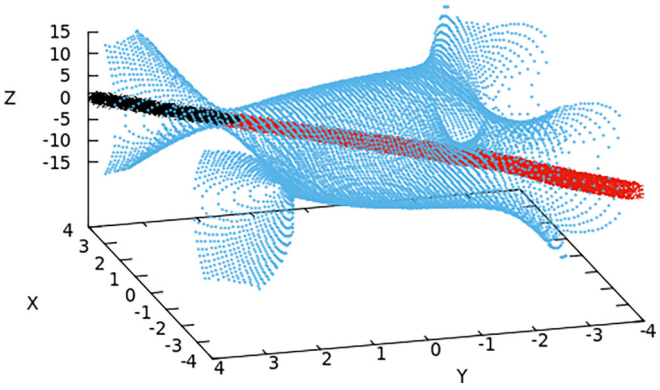

FIG. 2. The trajectories [with red (dark gray)color denoting forward in time] in the configuration space that have initial conditions on the dividing surface associated with the upper-right index-1 saddle. In this case, the trajectories move in the direction of the reaction. The trajectories (with black colordenoting backward in time) in the configuration space that have initial conditions on the dividing surface associated with the upper-right index-1 saddle. In this case, the trajectories do not move in the direction of the reaction (they belong to nonreactive part). The zero-velocity surface is depicted in cyan (light gray).

curve in the subspace (y, p_y). Then according to the algorithm (see more details in Ref. [31]) we construct a torus that is the result of the product of the projection (y, p_y) of the periodic orbit with a circle (with a radius r) in the (x, y) subspace of the phase space and with another circle (with a radius r) in the (y, z) subspace of the phase space. This torus will be three-dimensional in the 4D space (x, y, z, p_y). Then we add a segment (taking a range p_x between its maximum and minimum value) and the torus increases its dimensionality by one (see Refs. [27,31]). Finally, we compute the value p_z using the Hamiltonian of the system.

Using the method of periodic-orbit dividing surfaces, for $r = 0.1$ and $r = 0.4$, we can compute the reactive and nonreactive parts of the trajectories that start from the region of the upper index-1 saddles. The reactive part corresponds to the trajectories that move forward in time to the central area of the Caldera (they have a probability to cross the region of one of the lower index-1 saddles). On the contrary, the nonreactive part corresponds to the trajectories that forward in time go to infinity. For the results that are presented in Figures 2–5 we used the value $r = 0.1$ (the figures are similar for the case of $r = 0.4$). The reactive and nonreactive parts are composed of two categories of trajectories. These categories are determined from the behavior of the trajectories backward in time. The first category of the reactive part is represented by trajectories that backward in time go to infinity (see Fig. 2). The second category of the reactive part is represented by trajectories that backward in time go to the central area of the Caldera (see Fig. 3). Similarly, the first and second categories of the nonreactive part of the trajectories are represented by trajectories that backward in time move to the central area of the Caldera (see Fig. 4) and to infinity (see Fig. 5), respectively. The first category of reactive and nonreactive parts was expected and is found also in 2D cases of the Caldera potential-energy surface (see Refs. [16,17]). The second category of the reactive and

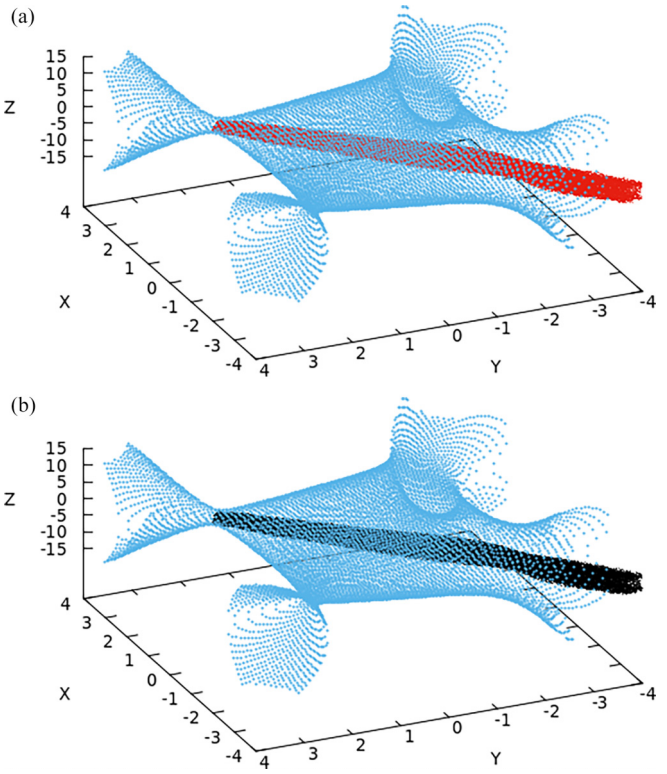

FIG. 3. (a) The trajectories [with red (dark gray) color denoting forward in time] in the configuration space that have initial conditions on the dividing surface associated with the upper-right index-1 saddle. In this case, the trajectories move in the direction of the reaction. The zero-velocity surface is depicted in cyan (light gray). (b) The trajectories (with black color denoting backward in time) in the configuration space that have initial conditions on the dividing surface associated with the upper-right index-1 saddle. In this case, the trajectories move in the direction of the reaction. The zero-velocity surface is depicted in cyan (light gray).

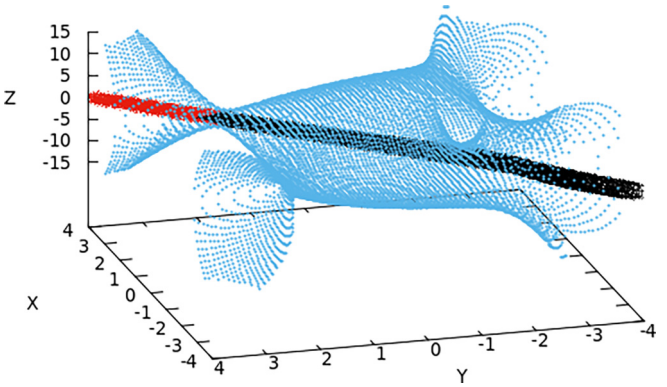

FIG. 4. The trajectories with red (dark gray) color (forward in time) in the configuration space that have initial conditions on the dividing surface associated with the upper-right index-1 saddle. In this case, the trajectories do not move in the direction of the reaction (they belong to the nonreactive part). The trajectories with black color (backward in time) in the configuration space that have initial conditions on the dividing surface associated with the upper right index-1 saddle. In this case, the trajectories move in the direction of the reaction. The zero-velocity surface is depicted in cyan (light gray).

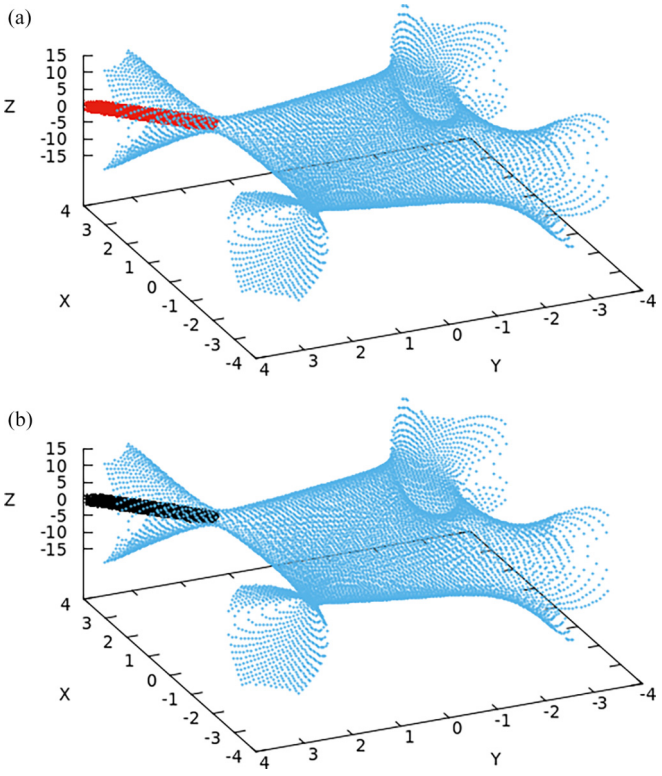

FIG. 5. (a) The trajectories [with red (dark gray) color denote forward in time] in the configuration space that have initial conditions on the dividing surface associated with the upper-right index-1 saddle. In this case, the trajectories do not move in the direction of the reaction (they belong to nonreactive part). The zero-velocity surface is depicted in cyan (light gray). (b) The trajectories (with black color denoting backward in time) in the configuration space that have initial conditions on the dividing surface associated with the upper-right index-1 saddle. In this case, the trajectories do not move in the direction of the reaction (they belong to the nonreactive part). The zero-velocity surface is depicted in cyan (light gray).

nonreactive parts was found only in 3D cases of the Caldera potential-energy surfaces and it is because of homoclinic intersections of invariant manifolds of NHIMs (see Ref. [31] for details).

We observe that all trajectories of the reactive part go straight across the Caldera and they exit through the region of the opposite lower index-1 saddle. This means that we have for our case the phenomenon of dynamical matching (as you can see also in Ref. [31]). Furthermore, we computed (for fixed values of radius $r = 0.1$ and $r = 0.4$) the reactive and nonreactive ratios (the ratios of reactant and nonreactant parts). These ratios are defined as the number of the trajectories of the reactive part (or the nonreactive part) over the number of the trajectories with initial conditions on the periodic-orbit dividing surfaces. These ratios will give us an approximation of the reaction rate. These ratios are 0.4820 and 0.5180 for $r = 0.1$ and 0.4985 and 0.5015 for $r = 0.4$.

At this point, a natural question arises about the dependence of reactive and nonreactive ratios on the radius r of the periodic-orbit dividing surfaces that we used. In order to answer this question, we computed these ratios varying the radius from values close to zero until a value where we start

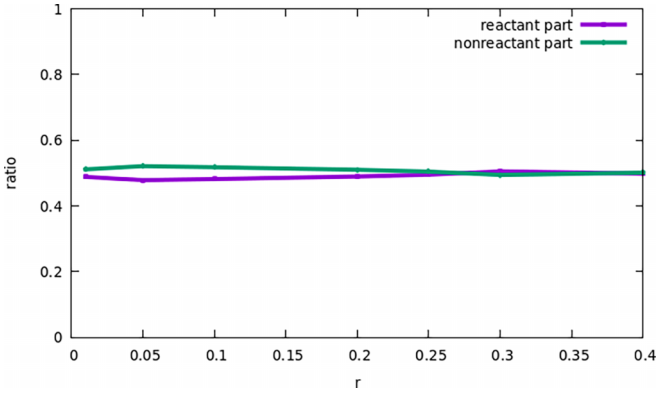

FIG. 6. The ratio of the trajectories that belong to the reactant part (purple curve) and the ratio of the trajectories that belong to the nonreactant part (green curve) versus the radius r of the periodic-orbit dividing surface. The purple curve (corresponding to the reactant part) can be fitted by the line 0.4912 and the green curve (corresponding to the nonreactant part) can be fitted by the line 0.5088.

to find a convergence of these ratios. In Fig. 6, we depict the reactive and nonreactive ratios versus the radius. We see that starting from a value of the radius close to zero, there are small fluctuations for small values of the radius and we see a convergence of these ratios for larger values of the radius. This means that the ratios of the reactant and nonreactant parts converge after a value of this radius (in our example more than 0.3), giving us a way to apply the method of periodic-orbit dividing surfaces in other nonintegrable Hamiltonian models. The curves for reactive and nonreactive ratios can be fitted by the lines $ratio = 0.4912$ and $ratio = 0.5088$, respectively. This means that the reactive and nonreactive ratios converge to values of 0.4912 and 0.5088, respectively. Furthermore, we observed that the initial fluctuations before the convergence of the ratios are very small, giving us a good approximation of the final value of the ratios (which corresponds to the values of the radius after the convergence).

IV. CONCLUSIONS

In a previous paper, we detected the phenomenon of dynamical matching in a 3D Caldera potential-energy surface. This was done in Ref. [31] using a method of the generalization of the periodic-orbit dividing surfaces in Hamiltonian systems with 3 degrees of freedom (see Refs. [27,28]) for a fixed value $r = 0.25$ of the radius of the periodic-orbit dividing surfaces. In this paper, we generalized these results by computing the reactive and nonreactive ratios for different values of r. We found a convergence of these ratios versus the radius of the periodic-orbit dividing surfaces and we presented the independence of the ratios from the radius of the periodic-orbit dividing surfaces.

ACKNOWLEDGMENTS

The authors acknowledge the financial support provided by EPSRC Grant No. EP/P021123/1. S.W. acknowledges the support of the William R. Davis '68 Chair in the Department of Mathematics at the United States Naval Academy.

[1] B. K. Carpenter, Trajectories through an intermediate at a fourfold branch point: Implications for the stereochemistry of biradical reactions, J. Am. Chem. Soc. **107**, 5730 (1985).

[2] B. Carpenter, Dynamic matching: The cause of inversion of configuration in the [1,3] sigmatropic migration? J. Am. Chem. Soc. **117**, 6336 (1995).

[3] J. Baldwin, Thermal rearrangements of vinylcyclopropanes to cyclopentenes, Chem. Rev. **103**, 1197 (2003).

[4] Z. Goldschmidt and B. Crammer, Vinylcyclopropane rearrangements, Chem. Soc. Rev. **17**, 229 (1988).

[5] C. Doubleday, K. Bolton, and W. Hase, Direct dynamics study of the stereomutation of cyclopropane, J. Am. Chem. Soc. **119**, 5251 (1997).

[6] C. Doubleday, M. Nendel, K. Houk, D. Thweatt, and M. Page, Direct dynamics quasiclassical trajectory study of the stereochemistry of the vinylcyclopropane-cyclopentene rearrangement, J. Am. Chem. Soc. **121**, 4720 (1999).

[7] C. Doubleday, C. Suhrada, and K. Houk, Dynamics of the degenerate rearrangement of bicyclo[3.1.0]hex-2-ene, J. Am. Chem. Soc. **128**, 90 (2006).

[8] M. Reyes, E. Lobkovsky, and B. Carpenter, Interplay of orbital symmetry and nonstatistical dynamics in the thermal rearrangements of bicyclo[*n*.1.0]polyenes, J. Am. Chem. Soc. **124**, 641 (2002).

[9] P. Collins, Z. Kramer, B. Carpenter, G. Ezra, and S. Wiggins, Nonstatistical dynamics on the Caldera, J. Chem. Phys. **141**, 034111 (2014).

[10] P. Pechukas and F. J. McLafferty, On transition-state theory and the classical mechanics of collinear collisions, J. Chem. Phys. **58**, 1622 (1973).

[11] P. Pechukas and E. Pollak, Trapped trajectories at the boundary of reactivity bands in molecular collisions, J. Chem. Phys. **67**, 5976 (1977).

[12] P. Pechukas and E. Pollak, Classical transition state theory is exact if the transition state is unique, J. Chem. Phys. **71**, 2062 (1979).

[13] P. Pechukas, Transition state theory, Annu. Rev. Phys. Chem. **32**, 159 (1981).

[14] E. Pollak and P. Pechukas, Transition states, trapped trajectories, and classical bound states embedded in the continuum, J. Chem. Phys. **69**, 1218 (1978).

[15] E. Pollak, Periodic orbits and the theory of reactive scattering, Theory Chem. React. Dyn. **3**, 123 (1985).

[16] M. Katsanikas and S. Wiggins, Phase space structure and transport in a Caldera potential energy surface, Int. J. Bifurcation Chaos **28**, 1830042 (2018).

[17] M. Katsanikas and S. Wiggins, Phase space analysis of the nonexistence of dynamical matching in a stretched Caldera potential energy surface, Int. J. Bifurcation Chaos **29**, 1950057 (2019).

[18] M. Katsanikas, V. J. García-Garrido, and S. Wiggins, The dynamical matching mechanism in phase space for Caldera-type potential energy surfaces, Chem. Phys. Lett. **743**, 137199 (2020).

[19] M. Katsanikas, V. J. García-Garrido, and S. Wiggins, Detection of dynamical matching in a Caldera Hamiltonian system using Lagrangian descriptors, Int. J. Bifurcation Chaos **30**, 2030026 (2020).

[20] Y. Geng, M. Katsanikas, M. Agaoglou, and S. Wiggins, The influence of a pitchfork bifurcation of the critical points of a symmetric Caldera potential energy surface on dynamical matching, Chem. Phys. Lett. **768**, 138397 (2021).

[21] Y. Geng, M. Katsanikas, M. Agaoglou, and S. Wiggins, The bifurcations of the critical points and the role of the depth in a symmetric Caldera potential energy surface, Int. J. Bifurcation Chaos **31**, 2130034(2021).

[22] S. Wiggins, L. Wiesenfeld, C. Jaffé, and T. Uzer, Impenetrable Barriers in Phase-Space, Phys. Rev. Lett. **86**, 5478 (2001).

[23] T. Uzer, C. Jaffé, J. Palacián, P. Yanguas, and S. Wiggins, The geometry of reaction dynamics, Nonlinearity **15**, 957 (2002).

[24] H. Waalkens, R. Schubert, and S. Wiggins, Wigner's dynamical transition state theory in phase space: classical and quantum, Nonlinearity **21**, R1 (2008).

[25] M. Toda, Dynamics of chemical reactions and chaos, Adv. Chem. Phys. **123**, 153 (2003).

[26] T. Komatsuzaki and R. S. Berry, Chemical reaction dynamics: Many-body chaos and regularity, Adv. Chem. Phys. 79 (2003).

[27] M. Katsanikas and S. Wiggins, The generalization of the periodic orbit dividing surface for Hamiltonian systems with three or more degrees of freedom in chemical reaction dynamics - I, Int. J. Bifurcation Chaos **31**, 2130028 (2021).

[28] M. Katsanikas and S. Wiggins, The generalization of the periodic orbit dividing surface for Hamiltonian systems with three or more degrees of freedom in chemical reaction dynamics - II, Int. J. Bifurcation Chaos **31**, 2150188 (2021).

[29] E. Wigner, The transition state method, Trans. Faraday Soc. **34**, 29 (1938).

[30] J. Reiff, J. Zatsch, J. Main, and R. Hernandez, On the stability of satellites at unstable libration points of sun–planet–moon systems, Commun. Nonlinear Sci. Numer. Simul. **104**, 106053 (2022).

[31] M. Katsanikas and S. Wiggins, The nature of reactive and non-reactive trajectories for a three dimensional Caldera potential energy surface, Phys. D (Amsterdam, Neth.) **435**, 133293 (2022).